Chapter 12
Reduced Order Structural Modeling for Control System Simulation

Max Dommers, Matthew S. Pearson, and Adam C. Johnson

Abstract Reduced order structural modeling is a highly effective tool for efficient system level simulation of mechanical systems. It has become heavily utilized in the aerospace industry for simulations that involve integration of a large number of subcomponent models or iteration across a large number of load cases. One common application is to incorporate flexible effects in an inertial body active control simulation. Industry examples of this include optical payload pointing simulation, space and aircraft GNC simulation, and fine robotic arm positioning. In these applications, flexible body dynamics are often considered secondary effects, but in many cases can have a substantial impact on performance. This study identifies a technical workflow for preparing a system level reduced-order structural model for efficient use in a closed-loop control simulation. The proposed procedure addresses common workflow challenges such as integrating multiple component models and converting the reduced model into a format usable in common coding languages. Further, the approach leverages previously established methods that retain model accuracy while reducing the degrees of freedom (DOFs) for efficient simulation. As an example problem, this study demonstrates the development of a flexible spacecraft structural plant model for optical pointing simulation. A broadly applicable approach is outlined for incorporating flexible body structural dynamics into control systems simulations.

Keywords State Space, Substructuring, Hurty/Craig-Bampton, Closed-loop control, Disturbance Rejection

Introduction

The baseline design of a controller for an inertial system focuses on guiding rigid body dynamics. High precision systems often require that the flexible body effects be considered in the finalized controller design. In the case of optical pointing or robotic arm control, seemingly miniscule vibrations can render the hardware ineffective at performing its designated task. Table 1 shows common control simulations that require assessment of flexible effects.

Table 1 Dynamic Control Simulations that May Require Flexible Body Representation

Engineering Problem	Rigid Representation	Impact of Flexible Body
Aerodynamic Steering	Aero forces acting on system inertia	IMU Vibration Feedback
Optical Pointing	Disturbance Forces acting on system inertia	Unwanted disturbance of chief ray (aka Jitter)
Robotic Arm Control	Joint motor forces acting on system inertia	Tool center point instability / vibration
Rocket / LV Steering	Thrust and aero forces acting on system inertia	IMU Feedback & Slosh instability

Though modern Finite Element Models (FEM) can offer accurate results, they are too computationally expensive to directly incorporate into a transient control simulation that may need to provide results quickly for tuning of controller

Max Dommers · Matthew S. Pearson · Adam C. Johnson
Quartus Engineering Incorporated, San Diego, CA 92121
e-mail: mdommers@quartus.com; matt.pearson@quartus.com; adam.johnson@quartus.com

© The Author(s), under exclusive license to River Publishers 2026
Kristin B. Zimmerman, PhD (eds.), *Special Topics & Experimental Techniques in Structural Dynamics, 2026, Vol. 5*, Conference Proceedings of the Society for Experimental Mechanics Series, https://doi.org/10.13052/rp-9788743814160

parameters through iteration or checking a large number of load cases. This problem can become even more prohibitive for system level simulations that involve combining models from multiple vendors amounting to large total DOF counts. Often times, simplifying dynamics models are incorporated to approximate flexible effects. Simplified flexible representations are sometimes used to alleviate this issue (e.g. mass spring models, pendulum models, simple flexible beam models, etc.). This report summarizes an approach for creating a reduced-order structural model that only retains a small number of DOFs without sacrificing model accuracy. The resulting model perfectly matches the response of an explicit coupled FEA system model. While the methods in this report are well established and based on common practice, the purpose of this work is to provide a single transparent guide for applying these methods specifically to the problem of controls modeling of dynamic systems.

Background

An example problem was developed based on the well-known ShockSat test article developed by Dr. Sam Yunis [13] for the purposes of sharing analysis and test results within the structural dynamics community. This article was chosen for this study because of its open source nature allowing transparent sharing of results. Further, the structure consists of two primary structural elements that resemble an optical payload and spacecraft bus structure, lending itself to demonstration of the line of sight (LoS) control problem. Figure 1 shows the FEA model that was previously developed of the ShockSat test article. In large spacecraft system level analysis, it is common for payload and bus vendors to be separate organizations, thus deliver models separately on independent timelines. To reflect this common logistical challenge, the Optical model and Spacecraft model were separated into two individual component models and reduced to a superelement in Hurty/Craig-Bampton (HCB) format before performing the study. The HCB format was selected for this study due to its common use in model sharing. However the described procedures will work on any mechanical system generally defined by a mass and stiffness matrix. A previous publication by Wender and Griebel [3] describes a general procedure for reducing a FEM in various software formats into this common HCB format from various independent FEA software suites.

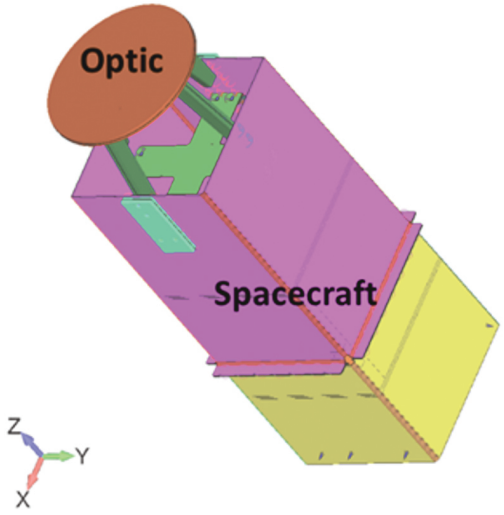

Fig. 1 FEA Model of ShockSat Test Article

Once the component models are assembled into a system level model and checked, the model can be used for rapid and efficient simulation. In this example, Figure 3 shows the key components of the coupled model for performing pointing error control simulation. The model allows motion of the dish structure to be recovered as an output due to 6 DOF disturbance forces applied to the frame of the structure. This input-output framework is analogous to a common jitter problem where operational noise from reaction wheels causes excessive pointing error in an imaging system. Figures 2 and 3 illustrate the assembly of the components that are used as inputs and outputs for this problem.

Finally, the Control Simulation section of this report shows how a reduced structural model like this can be installed into a control loop for the purposes of identifying issues in controller design and parameters during realistic operational load cases. In this report, only a single time domain control simulation is performed by incorporating a fast steering mirror (FSM) as a jitter mitigation approach.

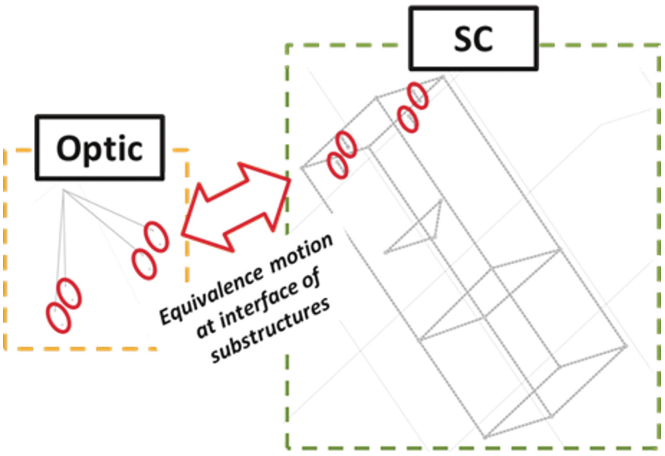

Fig. 2 Illustration of Coupling SC and Optic HCB Models at Interface DOFs

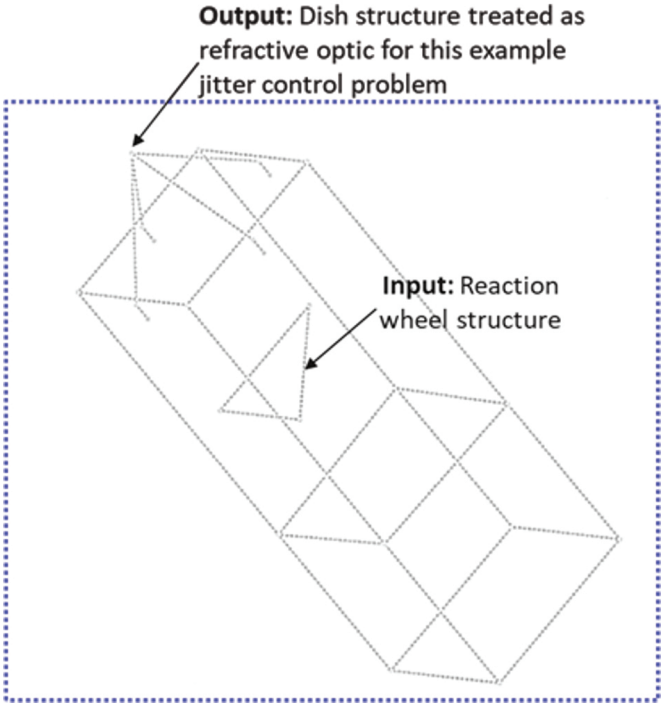

Fig. 3 Reduced ShockSat Model for Pointing Error Control Simulation

Component Mode Synthesis

In order to capture system-level dynamics properly, all component substructures must be connected at their respective interfaces. As a prerequisite for this work, it is assumed that the user has received all component models in Hurty/Craig-Bampton (HCB) format. This is a very common format for passing models efficiently among structural dynamics analysts particularly in the aerospace industry. The advantage to the HCB format is that it leverages the efficiency of a modal model while retaining physical degrees of freedom at the interface with other components. This allows for use of very small mass and stiffness matrices without substantial sacrifice in solution accuracy when compared to the explicitly modeled coupled system. A previous publication by Wender and Griebel [3] describes a general procedure for reducing a FEM into the common HCB format from various independent FEA software suites.

The initial component HCB models are treated as ordinary mass matrices (M_{HCB}), stiffness matrices (K_{HCB}), and damping matrices (Z_{HCB}) used in second order differential equations of motion as shown in (Equation 1).

$$[M_{HCB}]\{\ddot{P}\} + [Z_{HCB}]\{\dot{P}\} + [K_{HCB}]\{P\} = \{F\} \tag{1}$$

The mass, damping, and stiffness matrices have been transformed to take the form shown in (Equations 2-4), where ω is a diagonal matrix of constrained modal natural frequencies and various K and M terms define physical stiffness and mass at the boundaries and interfaces (B-Set) as well as cross terms between the boundaries and modal DOFs (Q-Set).

A few special considerations are noted. First, it is important to note that the B-Set of each component model should contain both the interface DOFs between the components as well as DOFs that are going to be used as inputs to the simulation. Second, this problem uses a simple modal damping formulation in which damping terms are only assigned to modal DOFs as shown in (Equation 4). This is common practice for simple structures, but other methods may be more appropriate for systems with non-homogenous or frequency dependent damping. In these cases, more tailored forms of component mode synthesis such as that of Hruda-Benfield [12] may be required.

$$[M_{HCB}] = \begin{bmatrix} M_{bb} & M_{bq} \\ M_{qb} & I \end{bmatrix} \tag{2}$$

$$[K_{HCB}] = \begin{bmatrix} K_{bb} & 0 \\ 0 & \omega^2 \end{bmatrix} \tag{3}$$

$$[Z_{HCB}] = \begin{bmatrix} 0 & 0 \\ 0 & 2\xi\omega \end{bmatrix} \tag{4}$$

Two HCB models are provided in this example, and they must be coupled together to form a single connected structure. The two structures will be called structure *a* and structure *b* respectively. Various approaches can be used to impose coupling constraints on components systems [1]. For this example, the rigid dual assembly method is used [2]. The first step is adding the HCB stiffness matrices of structure *a* and structure *b* to a single uncoupled stiffness matrix, $[K_{uncoupled}]$, as shown in (Equation 5).

$$[K_{uncoupled}] = \begin{bmatrix} K_{HCB,a} & 0 \\ 0 & K_{HCB,b} \end{bmatrix} \tag{5}$$

The coupling terms are added to the uncoupled stiffness matrix in the form of constraint equations for each coupled pair of DOFs. To create the constraint equations, corresponding DOFs to be coupled are identified. One from structure *a* and one from structure *b*. These two degrees of freedom are set equal as in (Equation 6).

$$p_a = p_b \tag{6}$$

The equation is rearranged such that it can be written into the stiffness matrix as show in (Equation 7). The augmented stiffness matrix shown in (Equation 8) now includes the constraint equation from (Equation 7) (now notated as "*CE*") and effectively enforces equivalence between the selected DOFs. This process is repeated for every DOF that needs to be linked between the two HCBs.

$$p_a - p_b = 0 \tag{7}$$

$$[K_{coupled}] = \begin{bmatrix} K_{HCB,a} & 0 & CE \\ 0 & K_{HCB,b} & -CE \\ CE & -CE & 0 \end{bmatrix} \tag{8}$$

The mass matrix is padded with zeros as shown in (Equation 9) to maintain the same size as the coupled stiffness matrix. This causes the mass matrix to be singular.

$$[M_{coupled}] = \begin{bmatrix} M_{HCB,a} & 0 & 0 \\ 0 & M_{HCB,b} & 0 \\ 0 & 0 & 0 \end{bmatrix} \tag{9}$$

The coupled damping matrix is created similarly to the mass matrix as shown in (Equation 10). This study assumes a 0.5% modal damping is applied to all modes.

$$[Z_{coupled}] = \begin{bmatrix} Z_{HCB,a} & 0 & 0 \\ 0 & Z_{HCB,b} & 0 \\ 0 & 0 & 0 \end{bmatrix} \tag{10}$$

Data recovery matrices (DRMs) are output transformation matrices describing the required transformation between HCB output and desired physical quantities. Any DRMs of the two HCB models are appended as shown in (Equation 11). Extra

zeros are added to the end of the DRM to ensure it has the same number of rows as the $[K_{coupled}]$, $[Z_{coupled}]$, and $[M_{coupled}]$ matrices.

$$[DRM_{coupled}] = [\ DRM_a \quad DRM_b \quad 0\ ] \tag{11}$$

Once a model is assembled, the component mode synthesis is verified by checking free-free modes of the coupled system. In general, there should be six rigid body modes of the system near zero Hz. If there are more, some components may not have been correctly connected. If there are less, the model may be grounded. In either case, the individual models and coupling equations should be checked for errors. Further, it is recommended that the DRM matrices contain sufficient output to visualize and verify rigid body motions and basic flexible modes of the coupled structure. Table 2 shows a free-free modes check for the ShockSat example problem. Though it is often not possible in practice, for this example the modes of the dual assembly component mode synthesis (right column) was compared against the explicitly assembled FEA model in Nastran (left column). The flexible modes agreed between the two methods within 0.001% and the rigid body modes were more than five orders of magnitude lower than the flexible modes in both cases.

Table 2 Free-free Modes Check

	Mode Frequency [Hz]		
	FEA Coupled	**Superelement After Dual Assembly**	**% Error**
Rigid Body Rx	3.221E-04	9.357E-05	N/A
Rigid body Tx	1.464E-04	2.180E-04	N/A
Rigid Body Rz	2.115E-04	3.462E-04	N/A
Rigid Body Ty	4.799E-04	3.617E-04	N/A
Rigid Body Ry	5.273E-04	3.917E-04	N/A
Rigid Body Tz	5.600E-04	4.528E-04	N/A
Axial 1	1.070E + 02	1.070E + 02	0.000%
X Bending 1	1.128E + 02	1.128E + 02	0.001%
Axial 2	1.149E+02	1.149E+02	0.000%
Y Bending 1	1.393E+02	1.393E+02	0.001%

State Space Conversion

For closed loop control simulations, a first order state space is typically desired for easy integration with other elements of the mechanical system. To achieve this form, the assembled second order system model is converted into the descriptor state space format shown in (Equation 12-13). It should be noted that the descriptor state space E matrix is only required due to the presence of a singular mass matrix (from the previous step). To avoid using the E matrix, the second order system can first be diagonalized and transformed into modal coordinates with mass normalized mode shapes. This will result in an identity E matrix allowing it to be neglected. Alternatively, different assembly methods may be used that avoid creating a singular mass matrix [1].

$$[E]\{\dot{x}\} = [A]\{x\} + [B]\{u\} \tag{12}$$

$$y = [C]\{x\} + [D]\{u\} \tag{13}$$

The second order equations of motion include the displacement column vector $\{P\}$ and it's second derivative $\{\ddot{P}\}$. The second order system is rewritten using a new state vector $\{x\}$. The top half of the state vector contains the displacement column vector $\{P\}$ and the lower half of the state vector contains the velocity column vector $\{\dot{P}\}$ as shown in (Equation 14).

$$\{x\} = \begin{Bmatrix} P \\ \dot{P} \end{Bmatrix} \tag{14}$$

The equations of motion from (Equation 1), with a damping matrix $[Z]$, is rewritten and reorganized using the state variable $\{x\}$ and its first derivative $\{\dot{x}\}$.

$$[M]\{\dot{x}\} = -[K]\{x\} - [Z]\{x\} + \{F\} \tag{15}$$

Once expanded, the previous equation takes this form shown in (Equation 16).

$$\begin{bmatrix} 0 & 0 \\ 0 & M \end{bmatrix} \begin{Bmatrix} \dot{P} \\ \ddot{P} \end{Bmatrix} = \begin{bmatrix} 0 & 0 \\ -K & -Z \end{bmatrix} \begin{Bmatrix} P \\ \dot{P} \end{Bmatrix} + \begin{Bmatrix} 0 \\ F \end{Bmatrix} \tag{16}$$

Note that the bottom half of (Equation 16) is a restatement of the equations of motion from (Equation 1). And the top half is empty. New equations that relate the derivative of the state vector to the state vector can fill the empty top half as shown in (Equation 17).

$$\begin{bmatrix} I & 0 \\ 0 & M \end{bmatrix} \begin{Bmatrix} \dot{P} \\ \ddot{P} \end{Bmatrix} = \begin{bmatrix} 0 & I \\ -K & -Z \end{bmatrix} \begin{Bmatrix} P \\ \dot{P} \end{Bmatrix} + \begin{Bmatrix} 0 \\ F \end{Bmatrix} \tag{17}$$

This is the first order descriptor state space form of the system where:

$$[E] = \begin{bmatrix} I & 0 \\ 0 & M \end{bmatrix} \tag{18}$$

$$[A] = \begin{bmatrix} 0 & I \\ -K & -Z \end{bmatrix} \tag{19}$$

$$[B] = \begin{Bmatrix} 0 \\ F \end{Bmatrix} \tag{20}$$

$$[C] = \begin{bmatrix} DRM_a & DRM_b & 0 \end{bmatrix} \tag{21}$$

$$[D] = 0 \tag{22}$$

And

$$[E]\{\dot{x}\} = [A]\{x\} + [B]\{u\} \tag{23}$$

$$y = [C]\{x\} + [D]\{u\} \tag{24}$$

Transfer Function Calculation

Now that the model is in state space format, various analyses can be performed. Frequency domain transfer functions are often desired to understand potential input frequencies that will cause excessive motion or feedback into a system. Transfer functions are the ratio of input to output in the frequency domain. In state space form, the state variable $\{x(t)\}$ and the input $\{u(t)\}$ are both functions of time. These equations can be converted into the complex frequency domain using the Laplace transformation.

$$[E]s\{X(s)\} = [A]\{X(s)\} + [B]\{U(s)\} \tag{25}$$

$$Y(s) = [C]\{X(s)\} + [D]\{U(s)\} \tag{26}$$

Rearranging and substituting the equations above will yield the equation to calculate transfer functions. If the model was transformed into modal coordinates before conversion into state space, then the descriptor matrix $[E]$ will be replaced by the identity matrix.

$$G(s) = C(Es - A)^{-1}B + D \tag{27}$$

Figure 4 shows an example of transfer function inspection for X axis reaction wheel disturbance to X axis optic displacement. This plot shows potentially problematic resonances in the structural system. Care must also be taken to recognize any modal truncation that has been applied to the model. In this case, modal response starts to roll off after 300 Hz. Though it is often not possible in practice, for this example the response of the reduced state space model (blue line) was compared against explicitly FEA simulation in Nastran. These two solutions overlay with no observable disagreement emphasizing the accuracy of the reduced model.

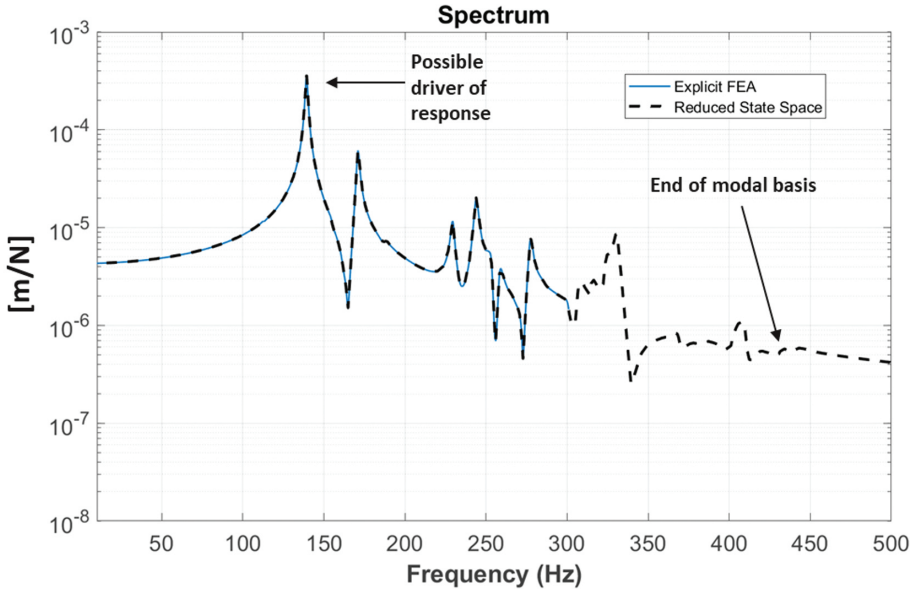

Fig. 4 Example Transfer Function Inspection Optic Tx / Reaction Wheel Fx

Control Simulation

A time domain simulation was created using Simulink to illustrate how the resulting state space model can be integrated into a control simulation. The ShockSat dish characterized previously is treated as the primary element of an optical system, in this case, a refractive lens. A simple optical payload consisting of a fast-steering mirror (FSM) and a generic sensing element are paired with the optic to represent a remote-sensing style optical system (see Figure 5). Typically, these types of systems utilize the FSM to steer the beam and reject optical jitter disturbances that may negatively impact the system's line of sight (LoS). The following section will demonstrate the rejection of disturbances from the onboard reaction wheel systems that impact system LoS using closed loop control.

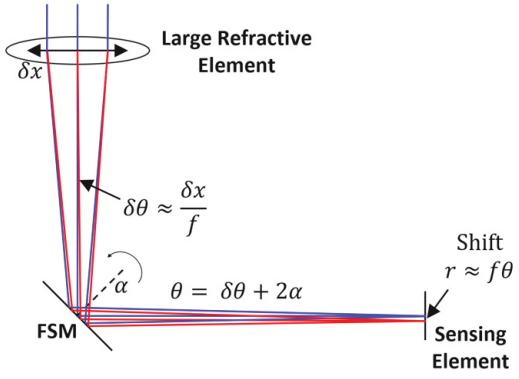

Fig. 5 Schematic of Simple Optical Payload for LoS Simulation

It is well known that for a thin lens, radial (or decenter) motions of the lens cause an angular steering of the output beam with respect to its nominal direction. To a first order linear approximation, this is the only impact to LoS [7]. Angular motions of the optic are insignificant to LoS and axial motion only causes a change in axial beam focus. As such, only the components of the state space model associated with the radial degrees of freedom, the disk x and y directions, need to be included in the simulation of this element. A small radial motion of the optic, δx, produces a beam tilt, $\delta\theta$, proportional to the inverse of the lens focal length [7].

$$\delta\theta = \frac{\delta x}{f} \tag{28}$$

For small motions of the flat FSM mirror, the change in the reflected light angle θ is related to the change in the mirror angle, α, by the following relationship [7]:

$$\theta = 2\alpha \tag{29}$$

At the sensing element, the deviation of the focused spot moves by the relationship:

$$r \approx f\theta = f(\delta\theta + 2\alpha) \tag{30}$$

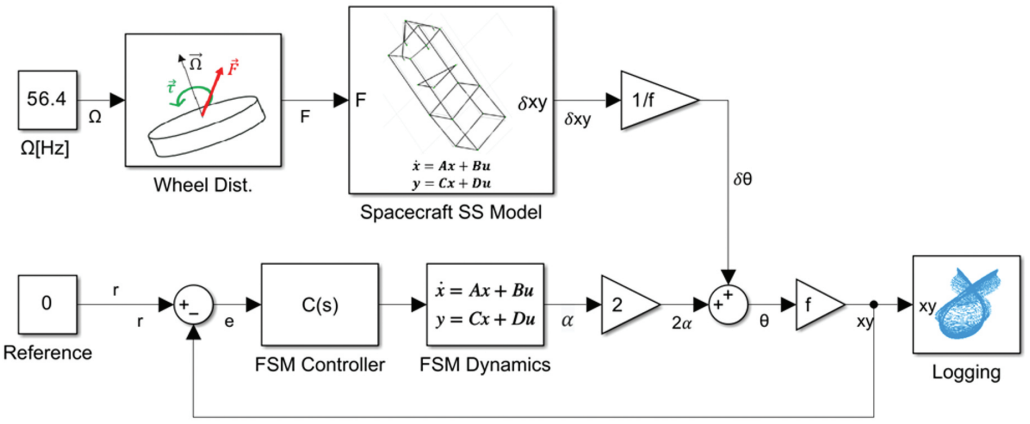

Fig. 6 LoS Pointing Simulink Model

The previous equations give the geometric relationship between the perturbed optics and the beam motion on the sensor. Now consider the components that interact dynamically with this geometric relationship. First, the FSM mechanism is considered. For the FSM model, idealized dynamics are assumed for simplicity, a simple 2nd order harmonic oscillator representation is used for each axis. While this is a simplification, other works have shown that this is a good approximation [10]. For both axes, the transfer function between the input voltage and the output FSM angle is:

$$T_x(s) = T_y(s) = \frac{\alpha(s)}{V(s)} = \frac{\omega_{FSM}^2}{s^2 + 2\xi_{FSM}\omega_{FSM}s + \omega_{FSM}^2} \tag{31}$$

This can be assembled into the 2x2 transfer function format:

$$\alpha_{FSM}(s) = \begin{bmatrix} \frac{\omega_{FSM}^2}{s^2+2\xi_{FSM}\omega_{FSM}s+\omega_{FSM}^2} & 0 \\ 0 & \frac{\omega_{FSM}^2}{s^2+2\xi_{FSM}\omega_{FSM}s+\omega_{FSM}^2} \end{bmatrix} V(s) \tag{32}$$

This can be represented in Simulink using either a transfer function or State Space form. The system was converted to State Space form from the transfer function using standard realization methods [6].

A simple proportional controller was used to stabilize the FSM. More sophisticated servo control schemes are possible but are unnecessarily complicated for this stable LoS pointing example and are left to future work.

$$C(s) = \begin{bmatrix} K_{px} & 0 \\ 0 & K_{py} \end{bmatrix} V(s) \tag{33}$$

To provide the disturbance input to the system, a single reaction wheel was modeled at one of the input positions of dynamic structural model. A common tonal disturbance model with harmonics proposed by Gutierrez [8][9] was used to capture realistic reaction wheel dynamics. This model computes the forces $\{m_{ij} | \ j = 1,2,3\}$ and moments $\{m_{ij} | \ j = 4,5,6\}$ of the ith wheel with the following equation:

$$m_{ij}(t) = \sum_{k=1}^{n_j} C_{ijk}\Omega_i^2 \sin(2\pi h_{jk}\Omega_i t + \phi_{ijk}) \tag{34}$$

where C_{ijk} is the amplitude of the kth harmonic, Ω_i is the frequency in Hz of the ith wheel, h_{jk} is the kth harmonic of the jth component of the ith wheel, and ϕ_{ijk} is the kth phase of the jth component of the ith wheel. To make sense mechanically,

it was assumed that the x and y components of the forces and moments have a phase difference of 90°. This is because the imbalance in the wheel is expected to be acting at different times in each direction as the wheel completes a full rotation.

Finally, the disturbance inputs are fed into the structural dynamic model and the outputs in the directions of the ShockSat dish are extracted:

$$\{\dot{x}\} = [\boldsymbol{A}]\{x\} + \begin{bmatrix} \boldsymbol{B_1} & B_{2,3,4} \end{bmatrix} \begin{Bmatrix} \boldsymbol{u_1} \\ u_{2,3,4} \end{Bmatrix} \tag{35}$$

$$y = \begin{bmatrix} C_{other} \\ \boldsymbol{C_{dish\ x.y}} \\ C_{dish\ z,rx,ry,rz} \end{bmatrix} \{x\} + \begin{bmatrix} D_{1\ other} & D_{2,3,4\ other} \\ \boldsymbol{D_{1\ dish\ x.y}} & D_{2,3,4\ dish\ x.y} \\ D_{1\ dish\ z,rx,ry,rz} & D_{2,3,4\ dish\ z,rx,ry,rz} \end{bmatrix} \begin{Bmatrix} \boldsymbol{u_1} \\ u_{2,3,4} \end{Bmatrix} \tag{36}$$

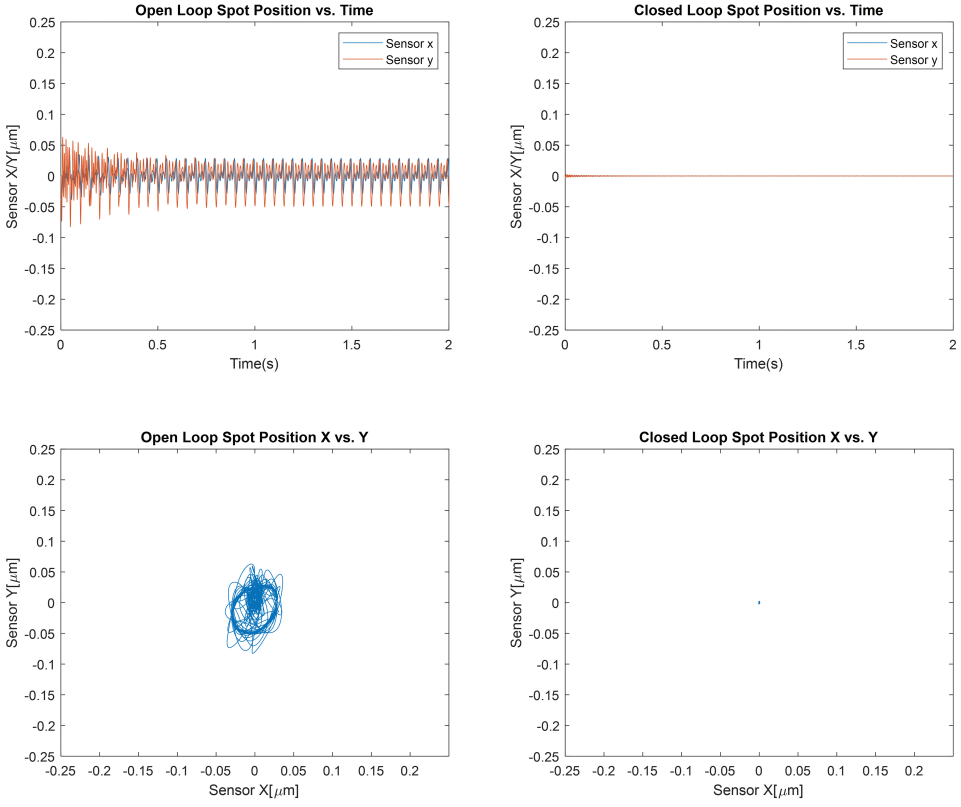

Fig. 7 Time and Spatial Domain Results for Ω_1= 20Hz

Selecting the necessary components for reaction wheel 1, and the dish x,y outputs, the following 6 input, 2 output MIMO state space model remains:

$$\{\dot{x}\} = [\boldsymbol{A}]\{x\} + [\boldsymbol{B_1}]\{\boldsymbol{u_1}\} \tag{37}$$

$$y = [\boldsymbol{C_{dish\ x.y}}]\{x\} + [\boldsymbol{D_{1\ dish\ x.y}}]\{\boldsymbol{u_1}\} \tag{38}$$

Note that the full A matrix is still used though further inspection of the states could allow for additional model reduction of A. Notably, the 1st mode of the full state space model at 107Hz is no longer present because it appears in the z axis direction only. The resulting output of this state space model, δxy, is divided by the focal length and added into the LoS equation as an output disturbance.

With all these sub-components, a complete LoS pointing model with structurally amplified output disturbances has been implemented. The disturbances are model output disturbances (rather than input disturbances) and as such, the controller can be tuned to attenuate the disturbance but only within the bandwidth of the controller.

The following parameters were used in the simulation:

Table 3 Simulation Parameters

Parameter Name	Value [Units]	Description
f	1.5 [m]	Optical System focal length
K_{px}, K_{py}	1800 [V/m]	Proportional Gain Factors
ω_{FSM}	100 [rad/s]	FSM axis natural frequency
ξ_{FSM}	0.3	FSM axis damping ratio
C_{ijk}	5x10^{-6} [N/Hz^2] [Nm/Hz^2] for $\{i = 1,2,3\}$	Tonal amplitude scale factor
h_{jk}	1,2,3	First 3 harmonics included
ϕ_{ijk}	$\{\phi_{i1k}, \phi_{i2k}, \phi_{i3k}, \phi_{i4k}, \phi_{i5k}, \phi_{i6k},\}$ = {0,90,0,0,90,0} [°]	Phases of each force/torque component

Results

Now that the model is constructed, there a few different ways it can be used to analyze the system's performance. By running the simulation in open loop and closed loop mode, it is possible to understand how effective the control system is at attenuating the disturbances. The results can be analyzed in a time domain, spatial domain, and frequency domain to assess closed loop performance.

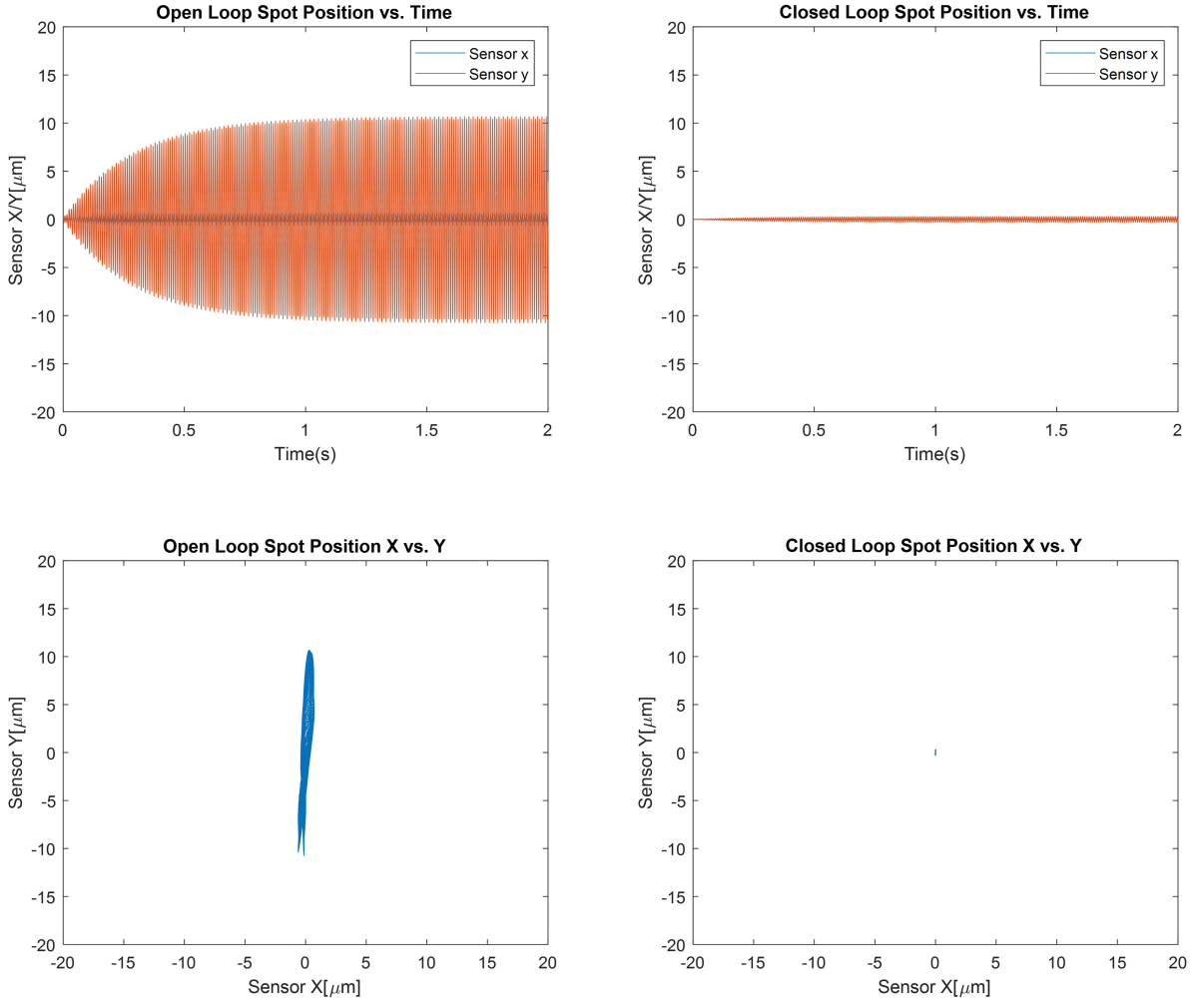

Fig. 8 Time and Spatial Domain Results for Ω_1= 56.4Hz (2nd harmonic at 1st x/y mode)

In the time domain, it is possible to see that sensor signals x and y are significantly less noisy with the presence of closed loop control. Pixel sizes on sensing element are often in the micron range. Submicron attenuation is achieved for this system using the simple closed loop controller proposed in the previous section. These results can also be analyzed in the spatial domain of x vs. y which is equivalent to the motion of the spot on the sensor. The open loop spot motion shows a limit cycle of large magnitude while the closed loop spot motion is significantly attenuated. As expected, there is a frequency dependent relationship between the wheel velocity and the rejected disturbances. It is useful to view this in the time domain to understand the absolute magnitude of the response, but the frequency dependent nature of the results is best understood in the frequency domain. This can be seen by computing the H_∞ norm of a frequency sweep across the structural model from the State space inputs to sensor measurement outputs and computing the singular values of the resulting frequency responses.[11]

The following plots show the frequency characteristics of the FSM control subsystem. The singular value plot shows a comparison of the worst case frequency response of the open loop and closed loop systems. Using the high bandwidth controller, it is possible to achieve meaningful attenuation at these high frequencies to reduce the LoS motion at the sensor.

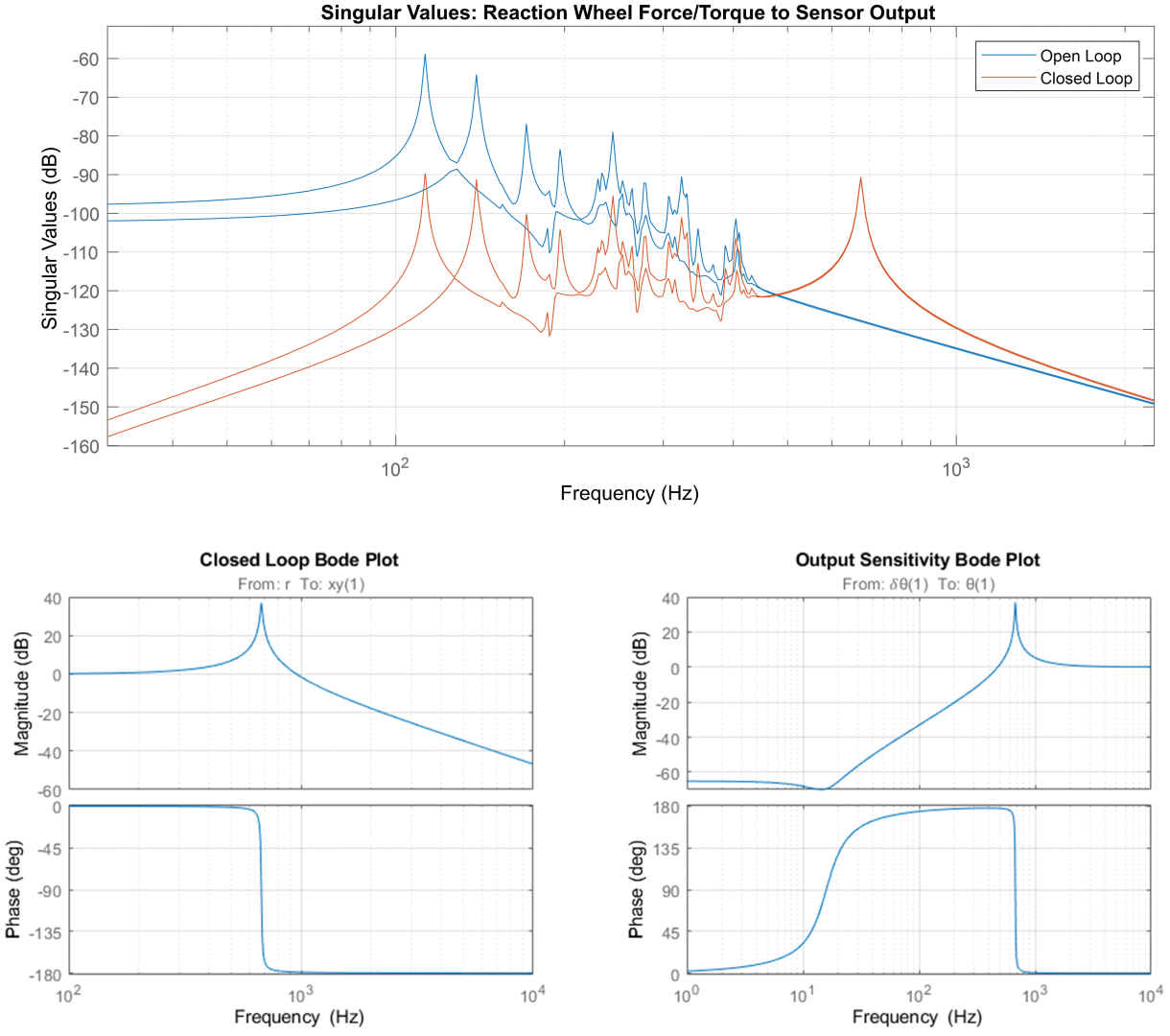

Fig. 9 Frequency Domain Results (top) Singular Value plot from force/torque input at reaction wheel to sensor measurement output, (bottom left) closed loop Bode plot of FSM control system, (bottom right) closed loop output sensitivity FSM control system

The closed loop Bode plot shows the closed loop response with a -3dB closed loop bandwidth around 1.05kHz. There is significant peaking at the 675Hz resonance frequency of the closed loop system. This peak also appears in the singular value plot on the far right side. The presence of this peak is a tradeoff of the closed loop approach. Further attenuation of this peak may be possible with additional control design or mechanical optimization of the FSM mechanism. Finally, the output sensitivity Bode plot shows the relationship between the output disturbance input to the control system and the measurement output as a function of frequency. Disturbances are significantly attenuated up to around 430Hz where the curve passes -3dB.

Conclusion

The outlined procedure successfully develops a reduced order system level structural model that can be efficiently utilized in closed loop time domain simulation of a mechanical system with a flexible structural element while retaining model accuracy. As an example, the outlined procedure is demonstrated on a spacecraft structure presented with the challenge of reducing optical pointing error due to structural vibration during operation. A system level spacecraft model is assembled from two component superelements. The coupled model passes basic checks and is shown to match the result when explicit FEA is used. The second order model is then converted to a first order state space representation for use in control system simulation. Frequency domain response inspection reveals potentially problematic resonances. The structural model is then integrated into a full system level control model and a controller is utilized to reduce the impact of the identified structural resonances. The functionality of the controller design is demonstrated through a closed loop time domain simulation of pointing error given a reaction-wheel-like disturbance input.

Acknowledgments
Dr. Ashkan Arianpour
Dr. Sam Yunis
Chris Flanigan

References

1. Kabe, Kabe, A. M. (2020). *Structural dynamics fundamentals and advanced applications: Volume II*. Academic Press.A. M. (2020).
2. Klerk, D. d. (2008). *General framework for dynamic substructuring: History, review, and classification of techniques*. AIAA.
3. Griebel, M., & Wender, T. (2025). *Software agnostic Hurty/Craig-Bampton dynamic model reduction*. In IMAC XLIV.
4. Scholz, H. (2015). *Control theory of descriptor systems lecture notes*. TU Berlin.
5. Li, Y., Green, T. C., & Gu, Y. (2024). *Descriptor state space modeling of power systems*. IEEE Transactions on Power Systems, 39(4), 5495-5508
6. Hespanha, J. P. (2018). *Linear systems theory* (2nd ed.). Princeton University Press.
7. Burge, J. H. (2006). *An easy way to relate optical element motion to system pointing stability. Current Developments In Lens Design And Optical Engineering VII, Proc. SPIE*, 6288, 62880I-1. DOI: 10.1117/OL.12.683809.
8. Gutierrez, H. L., Jr. (1999). *Performance assessment and enhancement of precision controlled structures during conceptual design* (Doctoral dissertation, Massachusetts Institute of Technology). Massachusetts Institute of Technology.
9. Liu, K.-C., Maghami, P., & Blaurock, C. (2008, August 18). Reaction wheel disturbance modeling, jitter analysis, and validation tests for Solar Dynamics Observatory (AIAA Paper No. 2008-7232). In *AIAA Guidance, Navigation, and Control Conference and Exhibit*.
10. Hawe, L. E. II. (2006). *Control of a fast steering mirror for laser-based satellite communication* (Master's thesis, Massachusetts Institute of Technology). Massachusetts Institute of Technology.
11. Zhou, K., & Doyle, N. (1998). *Essentials of robust control*. Prentice Hall, Inc.
12. Blelloch, P., & Tengler, J. C. (1998). *Application of Hruda-Benfield method to component damping for Space Shuttle coupled loads*. AIAA
13. Yunis, Sam. "ShockSat." NESC Academy Online, NASA Engineering and Safety Center, n.d., https://nescacademy.nasa.gov/workshops/ShockSat, Accessed 13 May 2026.